Diradicals, antiaromaticity, and the pseudo-Jahn-Teller effect: Electronic and rovibronic structures of the cyclopentadienyl cation

H. J. Wörner and F. Merkt

Citation: The Journal of Chemical Physics **127**, 034303 (2007); doi: 10.1063/1.2748049
View online: http://dx.doi.org/10.1063/1.2748049
View Table of Contents: http://scitation.aip.org/content/aip/journal/jcp/127/3?ver=pdfcov
Published by the AIP Publishing

Diradicals, antiaromaticity, and the pseudo-Jahn-Teller effect: Electronic and rovibronic structures of the cyclopentadienyl cation

H. J. Wörner and F. Merkt
Laboratorium für Physikalische Chemie, ETH-Zürich, 8093 Zürich, Switzerland

(Received 11 April 2007; accepted 16 May 2007; published online 17 July 2007)

The electronic and rovibronic structures of the cyclopentadienyl cation ($C_5H_5^+$) and its fully deuterated isotopomer ($C_5D_5^+$) have been investigated by pulsed-field-ionization zero-kinetic-energy (PFI-ZEKE) photoelectron spectroscopy and *ab initio* calculations. The vibronic structure in the two lowest electronic states of the cation has been determined using single-photon ionization from the $\tilde{X}\,^2E_1''$ ground neutral state and $1+1'$ resonant two-photon ionization via several vibrational levels of the $\tilde{A}\,^2A_2''$ excited state. The cyclopentadienyl cation possesses a triplet ground electronic state ($\tilde{X}^+\,^3A_2'$) of D_{5h} equilibrium geometry and a first excited singlet state ($\tilde{a}^+\,^1E_2'$) distorted by a pseudo-Jahn-Teller effect. A complete analysis of the $E\otimes e$ Jahn-Teller effect and of the $(A+E)\otimes e$ pseudo-Jahn-Teller effect in the $\tilde{a}^+\,^1E_2'$ state has been performed. This state is subject to a very weak linear Jahn-Teller effect and to an unusually strong pseudo-Jahn-Teller effect. Vibronic calculations have enabled us to partially assign the vibronic structure and determine the adiabatic singlet-triplet interval (1534 ± 6 cm^{-1}). The experimental spectra, a group-theoretical analysis of the vibronic coupling mechanisms, and *ab initio* calculations were used to establish the topology of the singlet potential energy surfaces and to characterize the pseudorotational motion of the cation on the lowest singlet potential energy surface. The analysis of the rovibronic photoionization dynamics in rotationally resolved spectra and the study of the variation of the intensity distribution with the intermediate vibrational level show that a Herzberg-Teller mechanism is responsible for the observation of the forbidden $\tilde{a}^+\,^1E_2'\leftarrow\tilde{A}\,^2A_2''$ photoionizing transition. © *2007 American Institute of Physics*. [DOI: 10.1063/1.2748049]

I. INTRODUCTION

The cyclopentadienyl cation ($C_5H_5^+$) is one of the prototypical molecules in the theory of aromaticity. Because of its four π electrons, it is usually considered to be antiaromatic but its diradical structure leads to several closely spaced electronic states that can be expected to have different structural, dynamical, and chemical properties.[1–4] The cyclopentadienyl cation is also a key molecule for the understanding of vibronic coupling effects including the Jahn-Teller (JT) and the pseudo-Jahn-Teller (PJT) effects.[5] The nature of the distortion of $C_5H_5^+$ and its origin have been discussed controversially in the literature[1,3] and a clarification of this situation is desirable.

Very little experimental information is available on the cyclopentadienyl cation. It has been observed by mass spectrometry[6,7] but neither optical nor photoelectron spectra have been reported yet. The spectroscopic information on $C_5H_5^+$ is currently limited to an electron-paramagnetic-resonance spectrum in a SbF_5 matrix which led to the conclusion that the ground electronic state is a triplet state with a small to negligible distortion from D_{5h} symmetry[8] but that a singlet state lies very close in energy.[9] The ordering of the lowest electronic states of $C_5H_5^+$ has been established in a preliminary report of our investigations of $C_5H_5^+$ by pulsed-field-ionization zero-kinetic-energy (PFI-ZEKE) photoelectron spectroscopy,[10] in which we have shown that the isolated cation possesses a triplet ground state of D_{5h} symmetry and that the lowest singlet state lies higher than the triplet ground state by less than 1600 cm^{-1}. The singlet state was found to possess a strongly distorted structure and low-frequency modes of nuclear motion. In the present article, we present a complete study of the PFI-ZEKE photoelectron spectra of the lowest singlet and triplet states of $C_5H_5^+$ and $C_5D_5^+$ recorded following single-photon excitation from the ground state and two-photon excitation via selected vibrational levels of the $\tilde{A}\,^2A_2''$ excited electronic state of the neutral radical. The spectra are assigned on the basis of vibronic coupling calculations using *ab initio* values of the coupling constants. The results show that the lowest singlet state of $C_5H_5^+$ is subject to a large PJT distortion and give insight into the complex nuclear motion in the manifold of strongly interacting electronic states. The vibrationally resolved measurements have been complemented by a set of rotationally resolved spectra which have enabled us to assign vibronic symmetries and determine the mechanism through which the $\tilde{a}^+\,^1E_2'\leftarrow\tilde{A}\,^2A_2''$ photoionizing transition, which is forbidden in the single-configuration approximation, draws its intensity.

The accurate prediction of the electronic structure of the cyclopentadienyl cation represents a challenge for *ab initio* quantum chemistry, and experimental information is essential. The electronic configuration $(\cdots)(a_2'')^2(e_1'')^2$ leads to three electronic states of symmetries $^3A_2'$, $^1E_2'$, and $^1A_1'$ in D_{5h} geometry. Most *ab initio* calculations,[1–3,11,12] but not all of them,[13] agree on the triplet being the ground electronic state

of $C_5H_5^+$. Calculated values for the adiabatic singlet-triplet interval vary from nearly zero to more than 7000 cm^{-1},[11] and recent values lie in the range of 1200–2500 cm^{-1}.[2,3] Investigations of the potential energy surfaces have shown that the $^1E_2'$ state is subject to a distortion leading to two structures of C_{2v} geometry and electronic symmetry $^1A_1$ lying very close in energy.[1–3,12] One of these structures is a minimum whereas the other is a first-order saddle point, but this property can be reversed depending on the level of *ab initio* theory and/or the basis set. Another stationary point with a C_{2v} geometry and a $^1B_2$ electronic symmetry has been identified by Lee and Wright[2] and shown to belong to the lowest singlet surface by Zilberg and Haas.[3]

In order to understand the nuclear dynamics in the manifold of interacting electronic states, it is essential to establish the topology of the potential energy surfaces and to construct a transparent model in terms of vibronic coupling theory. This approach has been pioneered by Köppel *et al.*[14] and has been successfully applied to a range of molecular systems that are closely related to $C_5H_5^+$.[15–17] Unfortunately, the knowledge of the potential energy surface of $C_5H_5^+$ remains incomplete and the relationship between the different stationary points has not been established unambiguously because the full symmetry of the vibronic problem has not been considered in most investigations. The fundamental implications of such topological properties on the nuclear dynamics have been discussed in several molecular systems[18,19] and are known in the more general context of the geometric phase.[20] The early work of Borden and Davidson[1] has been the most precise in this respect, showing that the origin of the stabilization of the $\tilde{a}^+\ ^1E_2'$ state of $C_5H_5^+$ is its vibronic coupling to the $^1A_1'$ state of the same electronic configuration. The effect was called a "second-order JT" effect but we prefer the expression "pseudo-Jahn-Teller" effect to distinguish it from the vibronic coupling effect within a degenerate state which is known as "quadratic" JT effect.[21] Borden and Davidson have also shown that the linear JT effect in the $\tilde{a}^+\ ^1E_2'$ state is very weak and would vanish in the absence of configuration interaction. Consequently, different kinds of electronic degeneracies are present on the lowest singlet potential surface of $C_5H_5^+$ and must be considered in the prediction of the nuclear dynamics. The theoretical strategy followed in the present article consists of a group-theoretical analysis of the vibronic coupling problem followed by *ab initio* calculations at the CASSCF level to determine approximate relative energies and vibronic coupling constants. This information is then used in a calculation of the vibronic structure which is compared to the experimental data.

II. THEORY

A. Electronic structure

The electronic structure of C_5H_5 and $C_5H_5^+$ at low energies can be understood qualitatively by considering the subset of molecular orbitals (a_2'', e_1'', and e_2'' in D_{5h} symmetry) associated with the π electron system. The $\tilde{X}\ ^2E_1''$ ground state and the $\tilde{A}\ ^2A_2''$ first excited electronic state of the neutral have configurations $(a_2'')^2(e_1'')^3$ and $(a_2'')^1(e_1'')^4$, respectively.

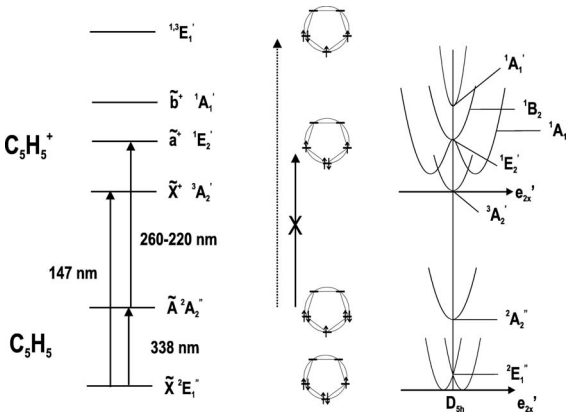

FIG. 1. One- and two-photon excitation schemes used to record photoionization and PFI-ZEKE photoelectron spectra of the cyclopentadienyl radical. The positions and symmetries of the low-lying electronic states of the cyclopentadienyl radical and cation are represented on the left-hand side of the figure by the horizontal lines and capital letters, respectively. The electronic configuration of the π molecular orbitals from which the electronic states derive are represented schematically in the central column. The right-hand side represents schematic cuts through the potential energy surface of the electronic states along nuclear displacements of e_2' symmetry.

Both states have been characterized by high-resolution spectroscopy.[16,17,22] The ground state is subject to a Jahn-Teller distortion along the e_2' modes.

The low-energy electronic configurations of $C_5H_5^+$ that derive from the π electron system and the corresponding states are

$$\text{(i)} = (a_2'')^2(e_1'')^2(e_2'')^0\text{: } {}^1A_1', \quad {}^3A_2', \quad {}^1E_2',$$

$$\text{(ii)} = (a_2'')^1(e_1'')^3(e_2'')^0\text{: } {}^1E_1', \quad {}^3E_1',$$

$$\text{(iii)} = (a_2'')^2(e_1'')^1(e_2'')^1\text{: } {}^1E_1', \quad {}^3E_1', \quad {}^1E_2', \quad {}^3E_2',$$

$$\text{(iv)} = (a_2'')^0(e_1'')^4(e_2'')^0\text{: } {}^1A_1'.$$

The configurations, electronic states, and potential curves that are relevant to our investigation of the photoelectron spectrum of C_5H_5 below 10 eV are represented schematically in Fig. 1 which shows on the left, middle, and right panels the ordering of the relevant electronic states, the corresponding configurations in the form of the usual Frost-Musulin diagrams, and one-dimensional schematic cuts through the potential energy surfaces along one component of an e_2' coordinate, respectively.

The three electronic states of the cation that result from the lowest electronic configuration $(a_2'')^2(e_1'')^2$ are represented schematically in Fig. 2. The Hartree-Fock energies of these three states at the D_{5h} geometry are

$$\begin{aligned} &{}^3A_2' \quad (2h + J_{23} - K_{23}), \\ &{}^1E_2' \quad (2h + J_{23} + K_{23}, 2h + J_{22} - K_{23}), \\ &{}^1A_1' \quad (2h + J_{22} + K_{23}), \end{aligned} \tag{1}$$

where h, J_{ij}, and K_{ij} represent the one-electron orbital energy, and the Coulomb and the exchange integrals, respectively, and the indices designate the π molecular orbitals of $C_5H_5^+$ in order of increasing energy.[23] By symmetry

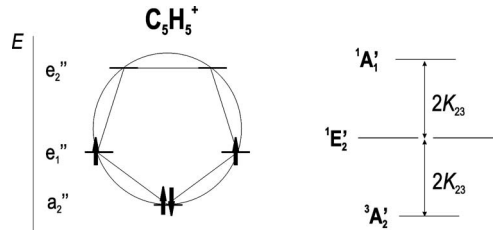

FIG. 2. Frost-Musulin diagram of the lowest-lying electronic configuration of the cyclopentadienyl cation (left-hand side) and energetic ordering of the corresponding electronic states in D_{5h} symmetry (right-hand side). K_{23} represents the exchange integral (see text).

$J_{22}-J_{23}=2K_{23}$ and hence the three states are equally spaced by $2K_{23}$. The lowest state is a nondegenerate triplet state because of the large value of the exchange integral.[1]

Consideration of the electronic configurations leads to the conclusion that single-photon ionization transitions to the ionic states associated with configurations (i) and (ii) are allowed from the $\tilde{X}\,^2E_1''$ ground state of the radical, whereas transitions to ionic states associated with configuration (i) are forbidden from the $\tilde{A}\,^2A_2''$ state. However, transitions to electronic states of configuration (i) may nevertheless be observed from the $\tilde{A}\,^2A_2''$ state if the interactions between configurations (i) and (ii) are significant. In particular, if the PJT interaction between the $^1E_2'$ and $^1A_1'$ states of configuration (i) is strong, the e_2' modes that mediate this interaction also lead to a mixing of the $^1E_2'$ state of configuration (i) with the $^1E_1'$ state of configuration (ii). This mechanism would facilitate the observation of the $^1E_2'$ ionic state from the $\tilde{A}\,^2A_2''$ neutral state and is now discussed in more detail.

B. Vibronic coupling

1. Potential energy surfaces

Since the diradical structure leads to electronic degeneracy and closely spaced electronic states, vibronic coupling must be considered. The D_{5h} symmetry of the system restricts the possible interactions. The $\tilde{a}^+\,^1E_2'$ state is subject to a Jahn-Teller effect. The symmetry of the inducing vibrational modes can be determined by group-theoretical methods[24,25] which we extend here beyond the second order.

For a vibrational mode to be JT active at the nth order in an electronic state of symmetry Γ_E, the symmetric nth power of its irreducible representation $[\Gamma_{\mathrm{JT}}]^n$ must be contained in the symmetric square of the electronic symmetry,

$$[\Gamma_E \otimes \Gamma_E] \supseteq [\Gamma_{\mathrm{JT}}]^n. \tag{2}$$

The condition for a nonvanishing nth-order PJT coupling between two electronic states of symmetries Γ_E and Γ_A is

$$\Gamma_E \otimes \Gamma_A \supseteq [\Gamma_{\mathrm{PJT}}]^n, \tag{3}$$

where Γ_{PJT} represents the irreducible representation of the PJT active vibrational mode. For the electronic states of relevance in the present study, the products of the electronic symmetries are $[E_2']^2=A_1'\oplus E_1'$ and $E_2'\otimes A_1'=E_2'$. Table I lists the symmetries of all modes that are JT or PJT active up to the fifth order in the present problem. Bilinear terms of the type $Q(e_1')Q(e_2')$ and $Q(e_1'')Q(e_2'')$, which are allowed in the second order of both the JT and PJT effects, have been disregarded in the derivation of the table. Although the role of such terms remains to be investigated in detail, they have been found both theoretically and experimentally to be negligible in C_5H_5.[16,17] One finds that linear JT active modes can only have symmetry e_1', linear PJT modes can only have symmetry e_2', quadratic JT modes are of symmetry e_2' or e_2'', and quadratic PJT modes of symmetry e_1' or e_1''. This alternation of linear and quadratic activity and the mutual exclusion of JT and PJT activity are general features of the groups possessing a C_n rotation axis with n odd and larger than 3 and leads to interesting topological properties of the potential energy surfaces.

TABLE I. Jahn-Teller and pseudo-Jahn-Teller activity of the doubly degenerate modes of the cyclopentadienyl cation up to fifth order.

Order	Γ_{vib}
JT activity in E_2'	
1	e_1'
2	e_2',e_2''
3	e_1',e_2'
4	e_1',e_2',e_1'',e_2''
5	e_1',e_2'
PJT activity $E_2'\leftrightarrow A_1'$	
1	e_2'
2	e_1',e_1''
3	e_1',e_2'
4	e_1',e_2',e_1'',e_2''
5	e_1',e_2'

Ceulemans[26] and Watson[27] have shown that the linear JT effect in a degenerate state arising from an $(e)^2$ configuration vanishes in the single-configuration approximation and therefore, the stabilization associated with the e_1' modes is expected to be small. This property had already been noticed by Borden and Davidson who demonstrated that the weak linear JT effect in the $\tilde{a}^+\,^1E_2'$ state of $C_5H_5^+$ has its origin in configuration interaction. They have also pointed out that the e_2' modes mediate a strong PJT interaction between the $\tilde{b}^+\,^1A_1'$ and the $\tilde{a}^+\,^1E_2'$ states which leads to a large stabilization of the lower component ($^1A_1$ in C_{2v}) of the $\tilde{a}^+\,^1E_2'$ state.

The Hamiltonian for nuclear motion in the coupled electronic manifold is most conveniently set up in a diabatic electronic basis, for which the matrix elements are smooth functions of the nuclear coordinates.[14] Using complex basis functions for the E state, the resulting Hamiltonian matrix H can be written as follows[15] (only linear terms are retained):

$$H = H^{\mathrm{PJT}} + H^{\mathrm{JT}}, \tag{4}$$

where

$$H^{\mathrm{PJT}} = h_0^{\mathrm{PJT}}\mathbf{1} + \begin{pmatrix} E_E & 0 & \sum_j \lambda_j r_j e^{i\phi_j} \\ 0 & E_E & \sum_j \lambda_j r_j e^{-i\phi_j} \\ H.c. & H.c. & E_A \end{pmatrix} \tag{5}$$

and

$$H^{\mathrm{JT}} = h_0^{\mathrm{JT}}\mathbf{1} + \begin{pmatrix} 0 & \sum_n g_n \rho_n e^{-i\theta_n} & 0 \\ H.c. & 0 & 0 \\ 0 & 0 & 0 \end{pmatrix}. \tag{6}$$

The degenerate vibrational modes mediating the vibronic coupling are described by cylindrical mass-weighted dimensionless normal coordinates r_j, ϕ_j, and ρ_n, θ_n, respectively. The first and second terms in Eq. (4) represent the PJT and JT interactions, respectively (H.c. means "Hermitian conjugate"). The harmonic oscillator terms h_0^{PJT} and h_0^{JT} in Eqs. (5) and (6) take the forms

$$h_0^{\mathrm{PJT}} = \sum_j \frac{\omega_j}{2}\left(-\frac{1}{r_j}\frac{\partial}{\partial r_j} r_j \frac{\partial}{\partial r_j} - \frac{1}{r_j^2}\frac{\partial^2}{\partial \phi_j^2} + r_j^2\right) \tag{7}$$

and

$$h_0^{\mathrm{JT}} = \sum_n \frac{\omega_n}{2}\left(-\frac{1}{\rho_n}\frac{\partial}{\partial \rho_n}\rho_n \frac{\partial}{\partial \rho_n} - \frac{1}{\rho_n^2}\frac{\partial^2}{\partial \theta_n^2} + \rho_n^2\right), \tag{8}$$

respectively. Although the adiabatic representation is of limited physical meaning in the case of strong vibronic coupling, it helps visualizing the topology and symmetry of the potential energy surfaces. The adiabatic potential surfaces are defined as the eigenvalues of the molecular Hamiltonian of Eq. (4), ignoring the nuclear kinetic energy. The adiabatic potentials have a simple appearance when only either JT or PJT displacements are considered. In the case of a single JT active mode with cylindrical coordinates (ρ, θ) the characteristic "Mexican-hat" potential of the E state is obtained,

$$V_{E^\pm}(\rho, \theta) = V_{E^\pm}(\rho) = V_E(0) + \frac{\omega_{\mathrm{JT}}}{2}\rho^2 \pm g\rho. \tag{9}$$

For a single PJT active mode with cylindrical coordinates (r, ϕ), two of the surfaces repel each other whereas the third remains unchanged. Assuming identical vibrational frequencies in the A and E states, the following potential surfaces are obtained:

$$V_A(r, \phi) = V_A(r) = \frac{V_E(0) + V_A(0)}{2} + \frac{\omega_{\mathrm{PJT}}}{2}r^2 + \sqrt{\left[\frac{V_A(0) - V_E(0)}{2}\right]^2 + 2\lambda^2 r^2},$$

$$V_{E^+}(r, \phi) = V_{E^+}(r) = V_E(0) + \frac{\omega_{\mathrm{PJT}}}{2}r^2, \tag{10}$$

$$V_{E^-}(r, \phi) = V_{E^-}(r) = \frac{V_E(0) + V_A(0)}{2} + \frac{\omega_{\mathrm{PJT}}}{2}r^2 - \sqrt{\left[\frac{V_A(0) - V_E(0)}{2}\right]^2 + 2\lambda^2 r^2}.$$

Both JT and PJT interactions lift the electronic degeneracy in the $\tilde{a}^+\,{}^1E_2'$ state but the effects are qualitatively different. Both e_1' and e_2' modes have two components e_x' and e_y'. A distortion along an e_x' component conserves C_{2v} symmetry,

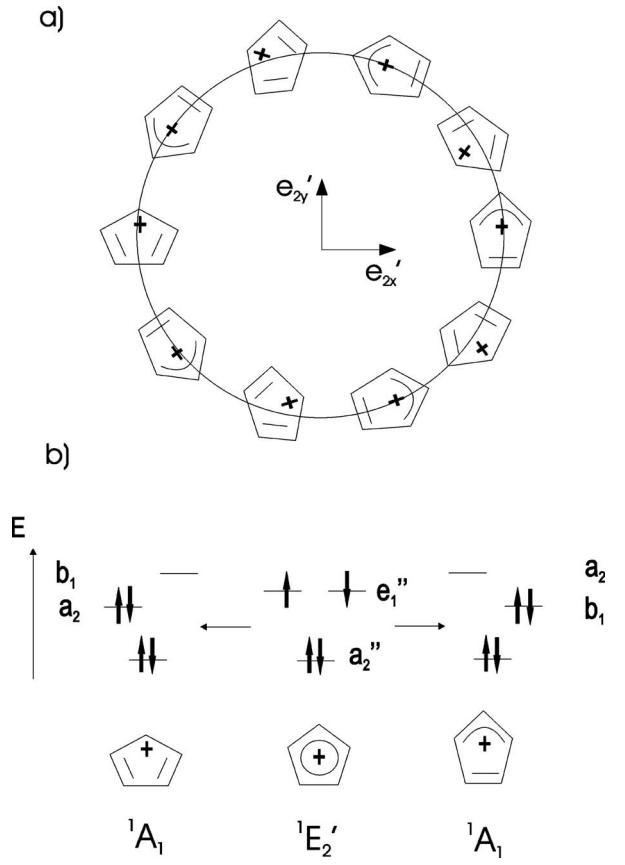

FIG. 3. (a) Schematic representation of the minimum energy pseudorotation path in the lowest singlet state. A distortion along the e_{2x}' dimension preserves C_{2v} symmetry and takes the molecule to either the allylic or dienylic structure. If vibronic coupling terms of third and higher orders are neglected, the displayed minimum energy path is isoenergetic. (b) Electronic configurations of the $\tilde{a}^+\,{}^1E_2'$ state at D_{5h} symmetry (middle) and of the distorted dienylic and allylic structures (left and right, respectively). The ordering of the a_2 and b_1 molecular orbitals originating from the degenerate e_1'' orbital is opposite in the dienylic and allylic structures.

whereas a distortion along an e_y' component lowers the symmetry to C_s. A distortion from D_{5h} to C_{2v} symmetry splits the $\tilde{a}^+\,{}^1E_2'$ state into two components of symmetries $^1A_1$ and $^1B_2$. In the case of a linear JT effect, the potential energy surfaces have a nonzero slope at the point of D_{5h} symmetry and, consequently, their ordering is reversed when the sign of the distortion coordinate is changed. In the case of a quadratic JT or a PJT effect, the slope of the adiabatic electronic surfaces vanishes at the point of highest symmetry and the ordering of the two components is independent of the sign of the distortion coordinate. In the present case, the lower component is totally symmetric ($^1A_1$ in C_{2v}) whereas the upper component has symmetry $^1B_2$ in C_{2v}.

These results can be generalized to include an arbitrary number of JT or PJT modes. The surfaces exhibit an overall rotational symmetry, i.e., they are invariant under the simultaneous substitutions[15]

$$\phi_j \rightarrow \phi_j - \alpha, \tag{11}$$

$$\theta_n \rightarrow \theta_n + 2\alpha. \tag{12}$$

This invariance reflects the existence of a vibronic angular momentum operator $\hat{\mathcal{L}}$ that commutes with the Hamiltonian

of Eq. (4) and is defined by[15]

$$\hat{\boldsymbol{\mathcal{L}}} = \hat{\ell}_{\text{vib}}\mathbf{1} + \hbar \begin{bmatrix} -1 & 0 & 0 \\ 0 & 1 & 0 \\ 0 & 0 & 0 \end{bmatrix}, \tag{13}$$

where

$$\hat{\ell}_{\text{vib}} = \frac{\hbar}{i}\sum_j \frac{\partial}{\partial \phi_j} - \frac{2\hbar}{i}\sum_n \frac{\partial}{\partial \theta_n}. \tag{14}$$

The existence of this constant of motion reflects the continuous symmetry of the vibronic coupling Hamiltonian of Eq. (4) and the quantum number associated with $\hat{\boldsymbol{\mathcal{L}}}$ can take any integer value. The inclusion of quadratic and higher-order vibronic coupling terms reduces this continuous symmetry to the molecular symmetry of the molecule under consideration.

In the case of the cyclopentadienyl cation, the D_{5h} symmetry requires that the linearly and quadratically active JT modes are different and that the e_2' PJT modes can only be quadratically JT active (see Table I). If vibronic coupling terms beyond the quadratic ones are neglected, the lower potential surface of the cyclopentadienyl cation possesses a one-dimensional isoenergetic subspace along the pseudorotation coordinate. The structures along this isoenergetic minimum energy path are displayed in Fig. 3(a) which is adapted from Ref. 1. The figure reveals that the allylic and dienylic structures that result from distortions along both directions of the e_{2x}' coordinate are isoenergetic and that the conversion from an allylic to a dienylic form is an equipotential process on the lowest singlet potential sheet. Upon distortion, the degenerate e_1'' orbitals are split in an a_2 and a b_1 orbital (in C_{2v} notation), the b_1 (a_2) orbital being energetically lowered (raised) when the distortion takes place along one direction of the e_{2x}' coordinate and raised (lowered) when it takes place along the other direction [see Fig. 3(b)]. Both distorted structures have C_{2v} symmetry and a $^1A_1$ ground state. This qualitative discussion will be made quantitative in Sec. IV A where the results of *ab initio* calculations are presented.

2. Dynamical calculations

The eigenstates of nuclear motion in the manifold of interacting electronic states are obtained by diagonalizing Hamiltonian (4) in a direct product basis of diabatic electronic functions and two-dimensional harmonic oscillator basis functions,

$$|\phi_k\rangle = |\Lambda\rangle \prod_i |v_i, \ell_i\rangle, \tag{15}$$

where $\Lambda = 0$ and $(-1, 1)$ for the $^1A_1'$ state and the two components of the $^1E_2'$ state, respectively, and v_i and ℓ_i are the vibrational quantum number and the vibrational angular momentum quantum number of the harmonic oscillator basis state, respectively. The index i runs over all degenerate vibrational modes that are included in the basis. The vibronic angular momentum quantum number j associated with these basis functions is

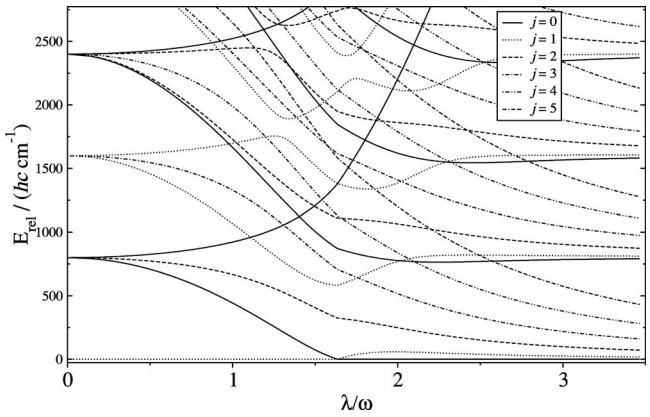

FIG. 4. Eigenvalues of the PJT Hamiltonian displayed as a function of the coupling parameter λ/ω assuming $\omega = 800$ cm^{-1}. The values are given with respect to the lowest level which is the doubly degenerate $j=1$ level for $\lambda/\omega < 1.6$ and the nondegenerate $j=0$ level for $\lambda/\omega > 1.7$.

$$j = \sum_i \ell_i + \Lambda, \tag{16}$$

and the matrix representation of the Hamiltonian of Eq. (4) is block diagonal in j, a property that can be exploited in the numerical calculations.

The eigenvalues possess a simple structure in the limit of very weak and very strong coupling. Figure 4 shows the eigenvalues of Hamiltonian (4) for a single PJT active vibrational mode with harmonic wave number $\omega = 800$ cm^{-1} in the range of $0 < (\lambda/\omega) < 3.5$ relative to the lowest level. The $^1A_1'$ state has been assumed to lie 5600 cm^{-1} above the $\tilde{a}^+\,^1E_2'$ state and a harmonic oscillator basis with vibrational quantum number up to $v = 100$ was used. In the limit of a vanishing coupling, the vibronic structure is that of a two-dimensional harmonic oscillator where each level has the degeneracy of $2(v+1)$. The ground vibronic state is thus doubly degenerate. As the coupling strength increases, the degeneracy of the vibronic levels is lifted and the resulting substates are singly ($j=0, A$ vibronic symmetry) or doubly ($j \geqslant 1, E$ or $A_1 \oplus A_2$ vibronic symmetry) degenerate. For sufficiently strong coupling, the $j=0$ level becomes the ground state thus leading to a transition from a doubly degenerate to a nondegenerate vibronic ground state. For values of $\lambda/\omega \geqslant 2$ the lowest vibronic levels converge to the simple structure of a one-dimensional rotor and the pattern repeats itself with the harmonic frequency of the PJT active vibration. This situation is similar to the strong-coupling limit of the $E \otimes e$ JT effect with the difference that the vibronic angular momentum quantum number is integer instead of half-integer. The emergence of the simple rotor structure is the result of the formation of a deep trough with cylindrical symmetry in the two-dimensional space of the e mode which results in a free pseudorotation around the trough and vibrations perpendicular to it. This situation also occurs in the B system of Na_3.[28–30]

The eigenvectors of the Hamiltonian (4) are linear combinations of the basis states of Eq. (15) with expansion coefficients a_k. The relative intensities of the vibronic bands in the photoelectron spectrum are calculated according to

$$I \propto \left| \left(\sum_k a_k \langle \phi_k | \right) \hat{\mu}_\alpha \left(\prod_{i'} |v_{i'}, \ell_{i'}\rangle \right) |\Lambda'\rangle \right|^2, \tag{17}$$

which separates to [see Eq. (15)]

$$I \propto \left| \left(\sum_k a_k \left[\prod_{i,i'} \langle v_i, \ell_i | v_{i'} \ell_{i'} \rangle \right] \langle \Lambda | \hat{\mu}_\alpha | \Lambda' \rangle \right) \right|^2. \tag{18}$$

In the calculations the overlap integral $\Pi_{i,i'}\langle v_i, \ell_i | v_{i'}\ell_{i'}\rangle$ from the intermediate $|\Lambda'\rangle\Pi_{i'}|v_{i'}\ell_{i'}\rangle$ level is assumed to be diagonal (i.e., $\langle v_i, \ell_i | v_{i'}\ell_{i'}\rangle = \delta_{v_i,v_{i'}}\delta_{\ell_i,\ell_{i'}}$). The simulation of the intensities thus depends on the transition moments to the diabatic components of $^1E_2'$ symmetry ($\Lambda=-1,1$) and $^1A_1'$ symmetry ($\Lambda=0$), for which we have used $\langle 1|\hat{\mu}_\alpha|\Lambda'\rangle = \langle -1|\hat{\mu}_\alpha|\Lambda'\rangle$ and $\langle 0|\hat{\mu}_\alpha|\Lambda'\rangle = 0$, as discussed below.

III. EXPERIMENT

The spectra were recorded using a tunable vacuum-ultraviolet (VUV) laser system coupled to a photoion time-of-flight mass spectrometer, a PFI-ZEKE photoelectron spectrometer,[31] and the pulsed source of jet-cooled radicals described in Ref. 32.

The cyclopentadienyl radicals were produced by photolysis of cyclopentadiene with the 248 nm output of a KrF excimer laser (Lambda Physik, CompEx) in a quartz capillary mounted at the end of a pulsed nozzle. The cyclopentadienyl radicals were cooled in the pulsed supersonic expansion into vacuum to rotational temperatures around 8 K. The supersonic beam was skimmed and then intersected by the VUV beam at right angles in the photoionization region. Cyclopentadiene was produced from dicyclopentadiene (Fluka) through distillation and stored at −78 °C until used. It was introduced in a stream of neat helium into the nozzle reservoir at a stagnation pressure of 5 bar.

Two excitation schemes were used and are illustrated in Fig. 1. The first consisted in single-photon VUV excitation from the ground state of the neutral radical to high Rydberg states located just below the rovibronic levels of the cation. The second scheme was a resonance-enhanced two-color two-photon excitation via selected vibrational levels of the $\tilde{A}\,^2A_2''$ state.

Tunable VUV radiation was generated by resonance-enhanced difference-frequency mixing ($\tilde{\nu}_{\mathrm{VUV}}=2\tilde{\nu}_1-\tilde{\nu}_2$) in krypton using the $(4p)^5(^2P_{3/2})5p[1/2]\ (J=0) \leftarrow (4p)^6\ ^1S_0$ two-photon resonance at $2\tilde{\nu}_1=94\,092.8632\ \mathrm{cm}^{-1}$. The frequency-tripled output ($\tilde{\nu}_1$) of a dye laser pumped by the second harmonic of a Nd:YAG laser (repetition rate 10 Hz; YAG denotes yttrium aluminum garnet) was kept fixed at the position of the two-photon resonance, and the VUV wave number was scanned by tuning the wave number $\tilde{\nu}_2$ of a second dye laser pumped by the same Nd:YAG laser. Before combining the two laser beams using a dichroic mirror and focusing them in a 30 cm long gold-coated cell filled with 15 mbar krypton, a telescope was used to prefocus the second laser so that the focal points of both beams coincided. A MgF_2 prism with an apex angle of 45° was employed to separate the VUV difference-frequency beam from the fundamental laser beams of wave numbers $\tilde{\nu}_1$ and $\tilde{\nu}_2$.

The resonance-enhanced two-photon excitation/ionization experiments were carried out using the (doubled) output of two dye lasers. The laser beams crossed the molecular beam at right angles in a counterpropagating arrangement. By scanning the first laser at a constant wave number of the second laser, spectra of the intermediate $\tilde{A}\,^2A_2''$ state were recorded. PFI-ZEKE photoelectron spectra were measured from selected vibrational levels of the $\tilde{A}\,^2A_2''$ level by fixing the wave number of the first laser at the appropriate spectral position and scanning the wave number of the second laser.

The rotationally resolved measurements were carried out using a Fourier-transform limited pulsed UV laser with a bandwidth of less than 200 MHz described in Ref. 33 in the first excitation step.

The wave number calibration of the spectra was achieved by simultaneously recording optogalvanic spectra of neon and making reference to tabulated transition wave numbers.[34]

The photoelectron spectra were recorded by monitoring the pulsed-field ionization of high Rydberg states ($n \gg 200$) as a function of the laser wave number using PFI-ZEKE photoelectron spectroscopy.[35] An electric field pulse sequence consisting of a discrimination pulse of +0.1 V/cm and a detection pulse of −0.4 V/cm delayed by 3 μs with respect to photoexcitation was used, resulting in a resolution of 1 cm^{-1}. A correction of 1.0 cm^{-1} was applied to compensate for the field-induced shift of the ionization thresholds. The photoionization spectra were obtained by measuring the $C_5H_5^+$ or $C_5D_5^+$ ion signal mass selectively as a function of the laser wave number. The ions were extracted using a pulsed electric field of 336 V/cm delayed by 200 ns with respect to the laser pulses.

IV. RESULTS

A. *Ab initio* calculations

The geometry of the $\tilde{X}^+\,^3A_2'$ state of $C_5H_5^+$ has been optimized at the CASSCF(4,5)/cc-pVTZ level of theory. The active space has been chosen to consist of the π molecular orbitals which are occupied by four electrons. The starting orbitals have been generated in a Hartree-Fock calculation of the cyclopentadienyl anion because $C_5H_5^-$ is a closed-shell molecule. The geometry optimization of the $\tilde{X}^+\,^3A_2'$ state led to a D_{5h} structure with a C–C bond length of 1.381 Å and a C–H bond length of 1.068 Å. The optimization was followed by a calculation of the vibrational normal modes and their frequencies which are listed in Table II for $C_5H_5^+$ and $C_5D_5^+$.

The electronic energy of the $\tilde{a}^+\,^1E_2'$ state was determined by optimizing the geometry of $C_5H_5^+$ at the D_{5h} conical intersection using the coupled-perturbed multiconfigurational self-consistent-field method implemented in MOLPRO.[36] The interval between the electronic minima of the $\tilde{X}^+\,^3A_2'$ and $\tilde{a}^+\,^1E_2'$ states at D_{5h} geometry was then calculated at the CASSCF(4,5)/cc-pVTZ level of theory. This quantity will subsequently be called the diabatic singlet-triplet interval and the calculated value is given in the top line of Table III. Table III also lists the energy intervals between the singlet states

TABLE II. Vibrational frequencies in the $\tilde{X}^+\,^3A_2'$ state of $C_5H_5^+$ and $C_5D_5^+$ calculated *ab initio* at the CASSCF(4,5)/cc-pVTZ level of theory.

Vibration	Symmetry	$C_5H_5^+$ ω/cm^{-1} [a]	$C_5D_5^+$ ω/cm^{-1} [a]
ν_1	a_1'	3065	2285
ν_2	a_1'	1063	1010
ν_3	a_2'	1286	1009
ν_4	a_2''	670	491
ν_5	e_1'	3054	2262
ν_6	e_1'	1389	1240
ν_7	e_1'	959	753
ν_8	e_1''	916	647
ν_9	e_2'	3054	2253
ν_{10}	e_2'	1420	1386
ν_{11}	e_2'	1075	828
ν_{12}	e_2'	803	722
ν_{13}	e_2''	824	778
ν_{14}	e_2''	423	352

[a]Scaled by multiplying the *ab initio* result with 0.90.

calculated after optimizing their (C_{2v}) geometry at the CASSCF(4,5)/cc-pVTZ level of theory and the $\tilde{a}^+\,^1E_2'$ and $\tilde{X}^+\,^3A_2'$ states calculated at the optimized D_{5h} geometry.

The optimization of the geometry of the singlet state in C_{2v} symmetry led to two different stationary points with a totally symmetric $(^1A_1)$ ground electronic state, which are represented in Fig. 5(a) and correspond to the dienylic (left) and the allylic structures (right) discussed in Sec. II B 1. At the CASSCF(4,5)/cc-pVTZ level of theory the allylic structure is found to be more stable than the dienylic structure by 320 cm^{-1} but the energetic ordering inverts at higher levels of theory and decreases below the accuracy of the calculations, as shown in Refs. 2 and 12. The geometry of $C_5H_5^+$ has also been optimized by requiring the electronic symmetry to be $^1B_2$. In this case, a different structure was obtained, that is represented schematically in Fig. 5(b).

These results are analyzed in panel (c) of Fig. 5 in terms of a linear JT effect along the e_1' modes (right-hand side) and a PJT effect along the e_2' modes (left-hand side) following the symmetry considerations of Sec. II. The figure depicts the calculated potential energies along effective e_2' and e_1' modes pointing from the D_{5h} geometry to the relevant minimum energy structures. The degeneracy point in both figures lies at the same energy and the state labels are given in C_{2v} symmetry. Since the stabilization of the $^1A_1$ component of the $\tilde{a}^+\,^1E_2'$ state $(\sim 3700-4000\ \mathrm{cm}^{-1})$ is much larger than that

TABLE III. Intervals between the lowest electronic states of $C_5H_5^+$. The first interval is given at the optimized D_{5h} geometry of the triplet state at the CASSCF(4,5)/cc-pVTZ level of theory. The energies of the singlet states in the last two intervals are evaluated after optimizing their geometry at the CASSCF(4,5)/cc-pVTZ level of theory.

Interval	ΔE (CASSCF(4,5))/ $(hc\ \mathrm{cm}^{-1})$
$E_{\min}(\tilde{a}^+\,^1E_2')-E_{\min}(\tilde{X}^+\,^3A_2')$	5580[a]
$E_{\min}(\tilde{a}^+\,^1E_2')-E_{\min}(^1B_2)$	230
$E_{\min}(^1A_1)-E_{\min}(\tilde{X}^+\,^3A_2')$	1410

[a]Average of the $^1A_1$ and $^1B_2$ components.

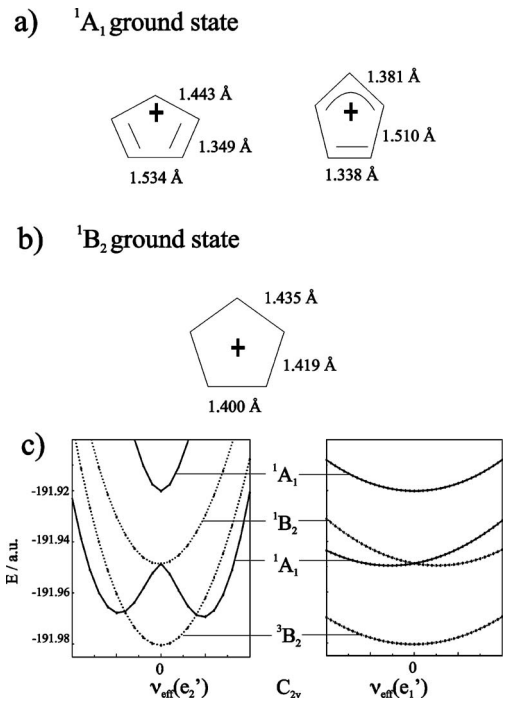

FIG. 5. (a) Structures obtained from geometry optimization at the CASSCF(4,5)/cc-pVTZ level of theory. The dienylic structure (left) corresponds to a first-order saddle point and the allylic structure (right) to a minimum at this level of theory. These structures result from a PJT distortion along an e_2' mode. (b) Minimum energy structure with a $^1B_2$ ground electronic state optimized at the same level of theory. This structure results from a JT distortion along an e_1' mode. (c) One-dimensional cuts through the potential energy surfaces of the states deriving from the $\tilde{X}^+\,^3A_2'$, $\tilde{a}^+\,^1E_2'$, and $\tilde{b}^+\,^1A_1'$ states of $C_5H_5^+$ at D_{5h} geometry. The cuts are displayed along effective modes of symmetry e_2' (left) and e_1' (right) connecting the D_{5h} points to the relevant minimum energy structures. The distortion modes preserve C_{2v} symmetry which is used to label the electronic symmetries.

of the $^1B_2$ component $(\sim 200\ \mathrm{cm}^{-1})$, the linear JT effect is almost negligible in $C_5H_5^+$ and indeed only leads to a small geometrical distortion [compare Figs. 5(a) and 5(b)]. It is important to realize that this situation differs from that encountered in less symmetrical molecular systems: In a recent study of the JT and PJT effects arising from e^2 configurations, Garcia-Fernandez *et al.*[37] have shown that in molecules with C_n and S_n symmetry axes with $n \leqslant 4$ glancing intersections of the kind depicted in Fig. 5(c) are not possible. They occur in the cyclopentadienyl cation because the higher symmetry causes the JT and PJT distortions to take place along distinct modes (see Table I).

The choice of normal modes in vibronic coupling problems is a delicate matter because the potential energy surfaces are far from being harmonic. Different choices have been suggested in the past, including normal modes from a state-averaged calculation at the conical intersection[16] and normal modes of the neutral ground state in the investigation of vibronic coupling in molecular cations by photoelectron spectroscopy.[15] In the present case, we have chosen to use the normal vibrational modes of the $\tilde{X}^+\,^3A_2'$ ground state of the cation because it is nondegenerate and well separated from excited triplet states. The calculations of the $\tilde{a}^+\,^1A_1$ potential energy curves were performed starting from the optimized D_{5h} geometry of the triplet ground state and distort-

TABLE IV. Harmonic frequencies ω, stabilization energies E_{stab}, and reduced PJT coupling constants λ/ω for the four vibrational normal modes of symmetry e_2' calculated at the CASSCF(4,5)/cc-pVTZ level of theory for $C_5H_5^+$ and $C_5D_5^+$ (see also text). The normal modes were obtained from a calculation of the $\tilde{X}^+\,^3A_2'$ state at the CASSCF(4,5)/cc-pVTZ level. The last two columns show the values obtained after adjustment to the experimental spectra.

Mode	ω/cm^{-1}	E_{stab}(CASSCF(4,5))/(hc cm^{-1})	λ/ω	ω/cm^{-1} [a]	λ/ω[a]
		$C_5H_5^+$			
ν_9	3054	<10			
ν_{10}	1420	1880	1.70	1460	1.61
ν_{11}	1075	580	1.08	1140	1.00
ν_{12}	803	600	1.28	820	1.24
		$C_5D_5^+$			
ν_9	2253	<10			
ν_{10}	1386	1960	1.82	1455	1.67
ν_{11}	828	900	1.59	810	1.48
ν_{12}	722	75			

[a]Adjusted to the spectrum.

ing it stepwise along the e_{2x}' components of the four normal modes of symmetry e_2'. At each geometry, a Hartree-Fock calculation of the anion was performed first, followed by a CASSCF(4,5) calculation of the $^3B_2$, $^1A_1$, and $^1B_2$ states (in C_{2v} symmetry).

The stabilization energies E_{stab} along the four modes of symmetry e_2' were determined for $C_5H_5^+$ and $C_5D_5^+$ and are summarized in Table IV. The coupling constants λ_i were determined as follows. The total stabilization energy E_{stab}^T in a multimode pseudo-Jahn-Teller problem is given by[14]

$$\begin{cases} E_{stab}^T = (e - \Delta E/2)^2/2e & \text{for } e \geqslant \Delta E/2 \\ E_{stab}^T = 0 & \text{for } e \leqslant \Delta E/2, \end{cases}$$

$$\text{with } e = 2\sum_i \frac{\lambda_i^2}{\omega_i}, \tag{19}$$

where ΔE is the energetic interval between the E and the A state at the undistorted geometry. The total stabilization energy amounts to 4170 cm^{-1} at the CASSCF(4,5)/cc-pVTZ level (see Table III). The sum of the stabilization energies obtained by calculating cuts of the potential energy surfaces along the modes of symmetry e_2' is smaller and amounts to 3060 cm^{-1} in $C_5H_5^+$ and 2935 cm^{-1} in $C_5D_5^+$ (see Table IV). The smaller values of the latter two quantities compared to the former one is attributed to anharmonicities in the potential energy surfaces which are not taken into account by the present potential model. The quantity $2(\lambda_i^2/\omega_i)$ corresponds to the contribution of each vibrational mode i to the total stabilization energy. In order to obtain values of λ_i that yield the correct total stabilization energy, Eq. (19) was used to calculate the quantity e corresponding to the *ab initio* value E_{stab}^T=4170 cm^{-1}, the calculated values of the harmonic frequencies ω_i of the $\tilde{X}^+\,^3A_2'$ state, and the calculated separation (ΔE=5600 cm^{-1}) between the $\tilde{a}^+\,^1E_2'$ and $\tilde{b}^+\,^1A_1'$ states at D_{5h} geometry. e was then partitioned among the active modes in proportionality of their calculated stabilization energy, yielding a contribution e_i for mode i. This procedure provided the *effective* coupling constants $\lambda_i=(\omega_i e_i/2)^{1/2}$ summarized in Table IV.

B. Symmetry considerations and geometric phase

In combination with the symmetry analysis of Sec. II B the results of the *ab initio* calculations show that the dominant mechanism for the stabilization of the $\tilde{a}^+\,^1E_2'$ state is a PJT coupling to the $\tilde{b}^+\,^1A_1'$ state mediated by the modes of symmetry e_2'. The distortion of $C_5H_5^+$ thus occurs in the eight-dimensional subspace of the e_2' modes and in this subspace, the lifting of the electronic degeneracy is of second order in the nuclear displacements, and the electronic degeneracy corresponds to a "glancing intersection." The linear JT effect takes place in the six-dimensional subspace of the e_1' modes in which the lifting of the degeneracy is linear. These considerations are important in view of assessing a possible geometric phase resulting from a closed loop around a conical intersection.[38] Although an explicit consideration of the geometric phase is not required in a dynamical calculation of the type performed in the present work, because all relevant electronic states are included, the concept of a phase is useful in several respects. When the stabilization energy is large compared to vibrational frequencies, the nuclear motion can be viewed as taking place on the lowest potential energy surface only, but the geometric phase must be included and can have a profound impact on the dynamics as mentioned earlier.[18,19] In the present case, the stabilization resulting from the PJT effect dominates over that resulting from the linear JT effect. Consequently, the nuclear motion in the lowest vibronic levels is confined to the space of the e_2' modes. This motion does not encircle any conical intersection and, therefore, no geometric phase is associated with it. The relevant nuclear configurations associated with the motion of $C_5H_5^+$ along the minimum energy path are represented schematically in Figs. 3 and 5.

C. Single-photon VUV photoionization and PFI-ZEKE photoelectron spectra

PFI-ZEKE photoelectron spectra of C_5H_5 and C_5D_5 have been recorded following single-photon excitation from the $\tilde{X}\,^2E_1''$ neutral ground state. Figures 6(a) and 6(b) show the VUV photoionization (dashed lines) and PFI-ZEKE photo-

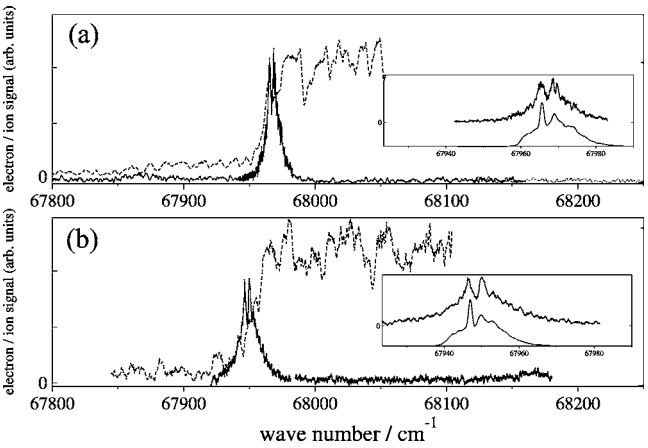

FIG. 6. One-photon VUV photoionization (dotted lines) and PFI-ZEKE photoelectron spectra (full lines) in the region of the adiabatic ionization threshold of $C_5H_5^+$ (a) and $C_5D_5^+$ (b) and simulations using a rotational temperature of 8 K for C_5H_5 and 12 K for C_5D_5 (insets). The spectra are assigned to the origin of the $\tilde{X}^+\,^3A_2' \leftarrow \tilde{X}\,^2E_1''$ transition.

electron spectra (full lines) of C_5H_5 and C_5D_5, respectively. The steps observed in both photoionization spectra at the position of the first band of each photoelectron spectrum mark the first adiabatic ionization thresholds. From a comparison with the two-color photoelectron spectra (see below), the photoelectron band is assigned to the transition to the vibrationless $\tilde{X}^+\,^3A_2'$ cationic ground state. Figure 6 also shows, in the insets, simulations of the rotational envelope of the first PFI-ZEKE photoelectron band of C_5H_5 and C_5D_5 using a rotational temperature of 8 K for C_5H_5 and 12 K for C_5D_5 and the orbital ionization model described in Refs. 39 and 40 assuming ionization from an orbital of d_π character. The simulation used the neutral ground state parameters from Refs. 22 and 41, Boltzmann population factors including spin-statistical weights and ionic rotational constants of the $\tilde{X}^+\,^3A_2'$ state from the *ab initio* equilibrium geometry determined at the CASSCF(4,5)/cc-pVTZ level of theory. We attribute the different rotational temperatures in the two spectra to slightly different experimental conditions. No further vibronic structure was observed in the spectral region of 67 800–71 500 cm^{-1} indicating almost diagonal Franck-Condon factors. Our sensitivity to PFI-ZEKE signal originating from the cyclopentadienyl radical was, however, reduced by the presence of strong hot and sequence bands of the precursor molecule (C_5H_6) covering the range above 68 280 cm^{-1}. A careful subtraction of the spectra recorded with and without photolysis did, however, not reveal any

TABLE V. Adiabatic ionization thresholds of the $\tilde{X}^+\,^3A_2' \leftarrow \tilde{X}\,^2E_1''$ and $\tilde{a}^+\,^1E_2' \leftarrow \tilde{X}\,^2E_1''$ photoionizing transitions of the cyclopentadienyl radical and first singlet-triplet interval $\Delta E(S_0\text{-}T_0)$ of $C_5H_5^+$.

	C_5H_5	C_5D_5	Literature
$IE(\tilde{X}^+\,^3A_2')/(hc\ cm^{-1})$	67967±4	67949±4	67830±800[a] (Ref. 6)
$IE(\tilde{a}^+\,^1E_2')/(hc\ cm^{-1})$	69501±4	69492±4	<69570 (Ref. 10)
$\Delta E(S_0\text{-}T_0)/(hc\ cm^{-1})$[b]	1534±6	1543±6	<1600 (Ref. 10)

[a]Value for C_5H_5.
[b]Adiabatic singlet-triplet interval in the cation.

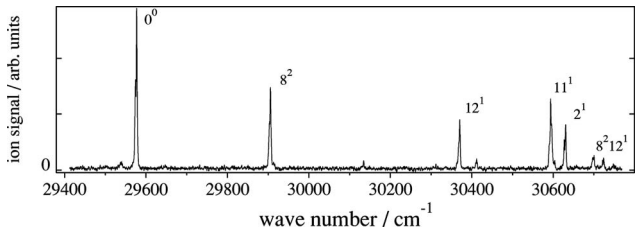

FIG. 7. Two-photon resonance-enhanced ionization spectrum of the $\tilde{A}\,^2A_2'' \leftarrow \tilde{X}\,^2E_1''$ transition of C_5H_5 with assignment of the vibrational structure.

vibrational structure that could be attributed to the cyclopentadienyl cation. The satisfactory agreement between the calculated and measured rotational contours of the origin band of the $\tilde{X}^+\,^3A_2' \leftarrow \tilde{X}\,^2E_1''$ transition suggests that the orbital ionization model captures the main features of the photoionization dynamics. It also permits the derivation of the accurate values of the adiabatic ionization energies of C_5H_5 and C_5D_5 given in Table V.

D. Photoionization and PFI-ZEKE photoelectron spectra recorded via the $\tilde{A}\,^2A_2''$ state

Photoionization and PFI-ZEKE photoelectron spectra have also been recorded using a $(1+1')$ two-photon excitation scheme via different vibrational levels of the $\tilde{A}\,^2A_2''$ intermediate state. The resonance-enhanced two-photon ionization spectrum of the $\tilde{A}\,^2A_2'' \leftarrow \tilde{X}\,^2E_1''$ transition of C_5H_5 is displayed in Fig. 7. The strong transitions observed in the spectrum are the same as those observed in the laser-induced fluorescence excitation spectrum reported in Ref. 17, but almost all weaker transitions observed in Ref. 17, several of which were assigned to hot and sequence bands, are absent from our spectrum. The vibrational temperature of the cyclopentadienyl radical thus appears to be lower in our experiment which suggests that vibrational degrees of freedom are more efficiently cooled in the expansion from the capillary into the high-vacuum region than in the experiment reported in Ref. 17 where the radicals were generated directly behind the nozzle. The assignments of the vibrational levels agree with those given in Ref. 17 which were derived from the analysis of dispersed fluorescence spectra.

The photoionization (dotted lines) and PFI-ZEKE photoelectron spectra (full lines) of C_5H_5 and C_5D_5 recorded following the $(1+1')$ two-photon resonant excitation via the ground vibrational level of the $\tilde{A}\,^2A_2''$ state are shown in Figs. 8(a) and 8(b), respectively. The spectra have been recorded from the origin of the $\tilde{X}^+\,^3A_2' \leftarrow \tilde{X}\,^2E_1''$ transition up to 4000 cm^{-1} of excess energy in the ions. The photoionization signal is zero at the position of the first adiabatic ionization energy but increases slowly over the lowest 1500 cm^{-1} and possesses several sharp resonances. A sharp increase of the photoionization signal is observed at the position of the strongest band in the PFI-ZEKE photoelectron spectrum of C_5H_5 (~69 572 cm^{-1}). The corresponding feature in the photoionization spectrum of C_5D_5 at 69 561 cm^{-1} is less

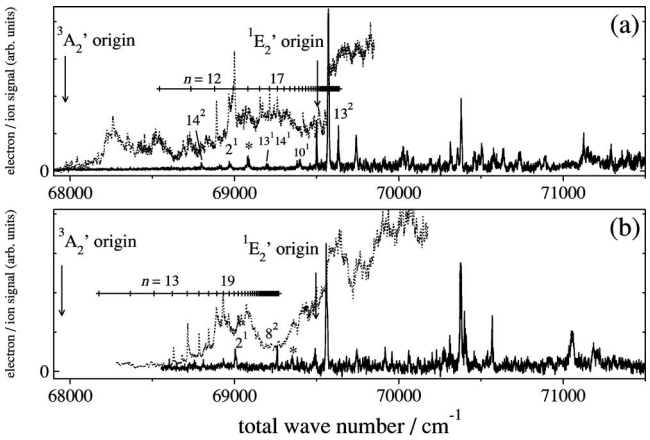

FIG. 8. Two-photon resonant photoionization and PFI-ZEKE photoelectron spectra (dotted and full lines, respectively) recorded via the vibrationless level of the $\tilde{A}\,^2A_2''$ state of C_5H_5 (panel a) and C_5D_5 (panel b). Vertical arrows mark the positions of the adiabatic ionization thresholds corresponding to the formation of the $\tilde{X}^+\,^3A_2'$ state and the lower component of the $\tilde{a}^+\,^1E_2'$ state. The horizontal lines with vertical assignment bars label autoionizing Rydberg series. The horizontal axis corresponds to the sum of the wave numbers of both lasers.

marked but still recognizable. In the photoionization spectrum of C_5D_5, seven resonances form a progression and are assigned to the members $n=13-19$ of an autoionizing Rydberg series [indicated in Fig. 8(b) by vertical lines on the assignment bar] with a small quantum defect and a series limit at 69 263 cm^{-1}. The corresponding ionization threshold is also observed in the PFI-ZEKE photoelectron spectrum which possesses a band at 69 261 cm^{-1}. In the photoionization spectrum of C_5H_5, the members $n=12-17$ of a less pronounced Rydberg series [labeled in Fig. 8(a)] converging to 69 634 cm^{-1} are observed. This ionization threshold corresponds to the position of the band in the PFI-ZEKE photoelectron spectrum located immediately above the strongest band.

The PFI-ZEKE photoelectron spectrum of C_5H_5 is dominated by the strong transition at 69 572 cm^{-1} which is accompanied by three weaker bands lying 71 cm^{-1} lower and 62 and 168 cm^{-1} higher. The lowest of these four bands is narrower than the upper three which all have a similar appearance. At higher wave numbers the spectrum possesses a second group of closely spaced lines around 70 380 cm^{-1}. The spacing and the relative intensities of the two strongest bands in this region are nearly identical to those of the two strongest bands around 69 572 cm^{-1}. Beyond this second group of lines, the spectral density and the widths of the observed bands increase. The separation between the most intense bands amounts to 808 cm^{-1} and the interval between the second group of lines and the broad structure at 71 120 cm^{-1} amounts to ~740 cm^{-1}.

A few weaker bands are also observed at lower wave numbers. The band marked with an asterisk could be assigned to the origin transition of the photoelectron spectrum of the precursor C_5H_6. This band was also observed in the absence of photolysis and disappeared when the laser pulse inducing the ionization was delayed with respect to the laser pulse inducing the $\tilde{A}\,^2A_2''\leftarrow\tilde{X}\,^2E_1''$ transition and is observed as a result of a nonresonant two-photon excitation process. The weak bands located between 68 500 and 69 700 cm^{-1} have been tentatively assigned to transitions to a totally symmetric fundamental (2^1), totally symmetric overtones and combination bands of out-of-plane vibrations ($14^2, 13^1 14^1, 13^2$) and the 10^1 level of the $\tilde{X}^+\,^3A_2'$ ground state of the cation by comparison with the calculated vibrational frequencies (see Tables II and VI).

The PFI-ZEKE photoelectron spectrum of C_5D_5 possesses less vibronic structure than that of C_5H_5. The dominant features are four bands located at 69561, 70377, 70568, and 71055 cm^{-1}. The overall intensity distribution and the intervals between the dominant features are similar to those observed in the spectrum of C_5H_5. A weak band is identified 70 cm^{-1} below the strongest band which matches the corresponding interval in the spectrum of C_5H_5. The band marked with an asterisk was also observed in the absence of photolysis and is therefore not attributed to $C_5D_5^+$. The weak bands located between 68 500 and 69 700 cm^{-1} have been tentatively assigned to transitions to a totally symmetric fundamental (2^1) and a totally symmetric overtone of an out-of-plane vibration (8^2) of the $\tilde{X}^+\,^3A_2'$ ground state of the cation by comparison with the calculated vibrational frequencies (see Tables II and VII).

To obtain more information on the complex spectral patterns observed between 69 500 and 71 500 cm^{-1}, additional PFI-ZEKE photoelectron spectra of C_5H_5 have been recorded via the vibrational levels 2^1, 11^1, and 12^1 of the $\tilde{A}\,^2A_2''$ state and are compared in Fig. 9. The spectrum recorded via the totally symmetric 2^1 level has a poor signal-to-noise ratio but its overall intensity distribution is similar to that of the spectrum recorded via the 0^0 level. The spectra recorded via the 11^1 and 12^1 levels have intensity distributions that differ strongly from those measured via 0^0 and 2^1. In both spectra, the band at 69 500 cm^{-1}, which coincides with a weak band in the spectra recorded via 0^0 and 2^1, is dominant. The two following bands at 69 572 and 69 632 cm^{-1} are also common to all four spectra but they are weak in the spectra recorded via the 11^1 and 12^1 intermediate levels. Two bands at 69 760 and 69 897 cm^{-1} are observed in the spectra recorded via the 11^1 and 12^1 levels which are not observed via the 0^0 or 2^1 levels. At higher wave numbers the spectra recorded via 11^1 and 12^1 begin to differ considerably from each other and from the spectra recorded via 0^0 and 2^1, and both possess a high spectral density. The bottom spectrum in Fig. 9 represents the PFI-ZEKE photoelectron spectrum of the precursor C_5H_6 which contributes weak lines to all spectra because of the weak nonresonant two-photon excitation mentioned above.

The $\tilde{A}\,^2A_2''\leftarrow\tilde{X}\,^2E_1''$ transition in C_5D_5 does unfortunately not give access to the 12^1 and 11^1 levels because of the weak JT activity of ν_{12} and its interaction with ν_{11}.[17] Therefore, PFI-ZEKE spectra could only be recorded via the vibrationally totally symmetric levels 8^2 and 2^1 and the corresponding spectra are shown in Fig. 10. The spectrum recorded via the 2^1 level shows the band at 69 561 cm^{-1} which

TABLE VI. Positions and assignments of vibronic bands in the PFI-ZEKE photoelectron spectra of C_5H_5. The total wave number with respect to the neutral ground state of the radical is indicated. The table also lists the wave numbers relative to the origins of the $\tilde{X}^+ {}^3A_2'$ and $\tilde{a}^+ {}^1E_2'$ ($^1A_1$ component) states and deviations between observed and calculated vibronic intervals.

$\tilde{\nu}_{obs}/(cm^{-1})$[a]	$[\tilde{\nu}_{obs}-IE(^3A_2')/(hc)]/(cm^{-1})$	$[\tilde{\nu}_{obs}-IE(^1E_2')/(hc)]/(cm^{-1})$	$(\tilde{\nu}_{obs}-\tilde{\nu}_{calc})/(cm^{-1})$	Assignment
68799	832		−6[b]	$\tilde{X}^+ {}^3A_2'$, 14^2 [c]
68974	1007		−56 [b]	$\tilde{X}^+ {}^3A_2'$, 2^1 [c]
69199	1232		−15 [b]	$\tilde{X}^+ {}^3A_2'$, $13^1\ 14^1$ [c]
69394	1427		7[b]	$\tilde{X}^+ {}^3A_2'$ 10^1 [c]
69501		0		$\tilde{a}^+ {}^1E_2'$ 0^0, $u=0$, $j=0$
69572		71	5	$\tilde{a}^+ {}^1E_2'$, $u=0$, $j=1$
69633	1666		18[b]	$\tilde{X}^+ {}^3A_2'$, 13^2 [c]
69740		239	−15	$\tilde{a}^+ {}^1E_2'$, $u=0$, $j=2$
69910				
70182				
70314				
70358		857	2	$\tilde{a}^+ {}^1E_2'$, $u=1$, $j=0$
70380		878	3	$\tilde{a}^+ {}^1E_2'$, $u=1$, $j=1$
70462				
70487				
70506				
70577		1076	−9	$\tilde{a}^+ {}^1E_2'$, $u=2$, $j=1$
70636				
70712				
70735		1234	9	$\tilde{a}^+ {}^1E_2'$, $u=3$, $j=1$
70852				
70890		1390	−4	$\tilde{a}^+ {}^1E_2'$, $u=4$, $j=1$
71125				
71148				

[a]Measured transition wave number without correction of the field-induced shift of the ionization thresholds.
[b]Harmonic wave numbers from *ab initio* calculations.
[c]Assignment tentative and on the basis of *ab initio* calculations.

was dominant in the other two spectra and the two bands at 70 377 and 70 405 cm^{-1} also observed via 0^0. The spectrum recorded via 8^2 shows in addition a weak band at 69 490 cm^{-1} and a satellite band to the higher wave number side of the main line. In all these cases, the intensity distributions are similar, as expected from the totally symmetric nature of the intermediate vibrational levels.

E. Rotationally resolved measurements

In order to assign the vibronic symmetry of the bands in the complex spectra of C_5H_5 reported in the preceding subsection, rotationally resolved PFI-ZEKE photoelectron spectra have been recorded using the $1+1'$ two-photon excitation scheme. For this purpose, the $\tilde{A}\ ^2A_2'' \leftarrow \tilde{X}\ ^2E_1''$ transition was

TABLE VII. Positions and assignments of vibronic bands in the PFI-ZEKE photoelectron spectra of C_5D_5. The total wave number with respect to the neutral ground state of the radical is indicated. The table also lists the wave numbers relative to the origins of the $\tilde{X}^+ {}^3A_2'$ and $\tilde{a}^+ {}^1E_2'$ ($^1A_1$ component) states and deviations between observed and calculated vibronic intervals.

$\tilde{\nu}_{obs}/(cm^{-1})$[a]	$[\tilde{\nu}_{obs}-IE(^3A_2')/(hc)]/(cm^{-1})$	$[\tilde{\nu}_{obs}-IE(^1E_2')/(hc)]/(cm^{-1})$	$(\tilde{\nu}_{obs}-\tilde{\nu}_{calc})/(cm^{-1})$	Assignment
69 007	1058		48[b]	$\tilde{X}^+ {}^3A_2'$, 2^1 [c]
69 261	1311		17[b]	$\tilde{X}^+ {}^3A_2'$, 8^2 [c]
69 491		0		$\tilde{a}^+ {}^1E_2'$, 0^0, $u=0$, $j=0$
69 561		70	4	$\tilde{a}^+ {}^1E_2'$, $u=0$, $j=1$
69 744		253	1	$\tilde{a}^+ {}^1E_2'$, $u=0$, $j=2$
699 17				
70 063				
70 312				
70 377		886	1	$\tilde{a}^+ {}^1E_2'$, $u=1$, $j=1$
70 406				
70 568		1077		$\tilde{a}^+ {}^1E_2'$, 2^1
71 054		1563	7	$\tilde{a}^+ {}^1E_2'$, $u=3$, $j=1$
71 195		1563	−11	$\tilde{a}^+ {}^1E_2'$, $u=4$, $j=1$

[a]Measured transition wave number without correction of the field-induced shift of the ionization thresholds.
[b]Harmonic wave numbers from *ab initio* calculations.
[c]Assignment tentative and on the basis of *ab initio* calculations.

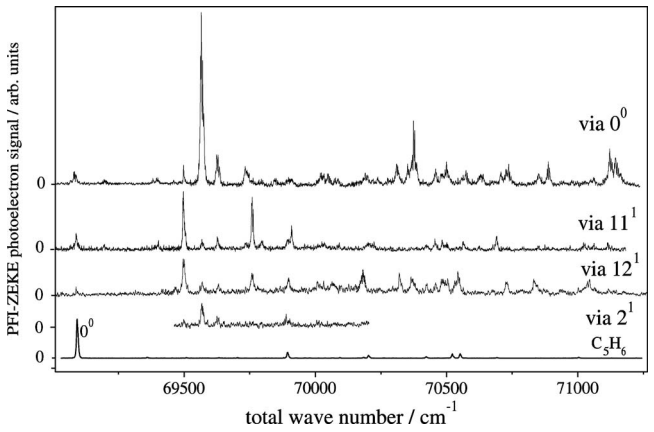

FIG. 9. PFI-ZEKE photoelectron spectra of C_5H_5 recorded following two-photon resonant excitation via selected vibrational levels of the $\tilde{A}\,^2A_2''$ state. The selected intermediate levels are indicated on the right-hand side above the spectra. The horizontal axis corresponds to the sum of the wave numbers of both lasers. The lowest trace is the PFI-ZEKE spectrum of cyclopentadiene (C_5H_6) recorded following single-photon VUV excitation from the neutral ground state.

pumped by a narrow-bandwidth ultraviolet laser[33] which allowed the excitation of single rotational levels of the $\tilde{A}\,^2A_2''$ 0^0 state. The rotationally resolved two-photon resonant ionization spectrum of the $\tilde{A}\,^2A_2''$ $0^0 \leftarrow \tilde{X}\,^2E_1''$ transition of C_5H_5 is displayed in Fig. 11. The spectrum has been analyzed and assigned previously in Ref. 22. The simulation of the spectrum based on the parameters and the Hamiltonian given in Ref. 22 and a temperature of 8 K is in quantitative agreement with the experimental results, as illustrated by the inset which compares the experimental spectrum (upper trace) with the simulated spectrum (lower trace).

Rotationally resolved PFI-ZEKE photoelectron spectra of the region of the strongest band of the PFI-ZEKE photoelectron spectrum around 69 572 cm^{-1} recorded via the intermediate levels $(N,K)=(1,0)$, (3,0), and (5,0) of the $\tilde{A}\,^2A_2''$ 0^0 state are shown in Fig. 12. For a direct comparison of the rotational structure the spectra have been shifted by the energy of the intermediate level. The vertical dotted lines mark the calculated positions of the $N^+=1-10$, K^+ levels using the

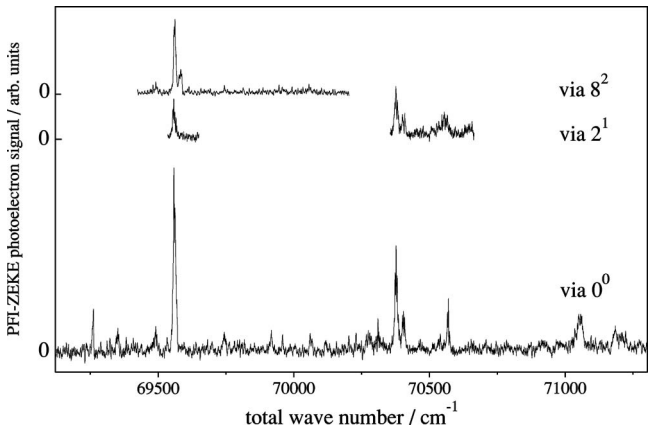

FIG. 10. PFI-ZEKE photoelectron spectra of C_5D_5 recorded following two-photon resonant excitation via selected vibrational levels of the $\tilde{A}\,^2A_2''$ state. The intermediate levels are indicated on the right-hand side. The horizontal axis corresponds to the sum of the wave numbers of both lasers.

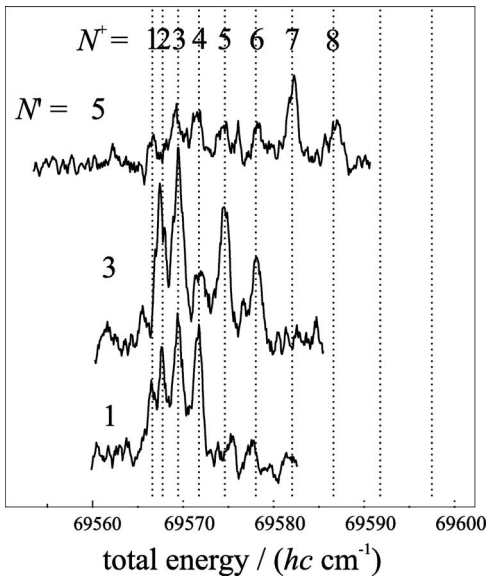

FIG. 12. Rotationally resolved PFI-ZEKE photoelectron spectra of C_5H_5 recorded following two-photon resonant excitation via selected rotational levels $(N',K'=0)$ of the vibrationless level of the $\tilde{A}\,^2A_2''$ state. The values of the total angular momentum quantum number (excluding spins) N' of the intermediate level and N^+ of the ionic level are indicated on the left-hand side and top, respectively. The horizontal axis corresponds to the total wave number above the $(N''=0,\ K''=0)$ level of the $\tilde{X}\,^2E_1''$ ground state.

rotational constant $B=0.286$ cm^{-1} for the D_{5h} geometry of the $\tilde{a}^+\,^1E_2'$ conical intersection. The comparison of the observed and predicted line positions shows that the ionic levels $N^+=1,2,3,4$ are accessed from the (1,0) intermediate state, the levels $N^+=2-6$ from the (3,0) level, and the levels $N^+=3-8$ from (5,0). The value of K^+ cannot be determined unambiguously because levels differing in K^+ lie too close to each other to be resolved at low values of K^+. Moreover, the spacings of rotational levels within a K^+ stack are equal in the symmetric top approximation. The analysis of these spectra thus requires the consideration of photoionization selection rules.

The intermediate levels used in this experiment are of A_1'' rovibronic symmetry. The rovibronic photoionization selection rules[42] in D_{5h} symmetry are

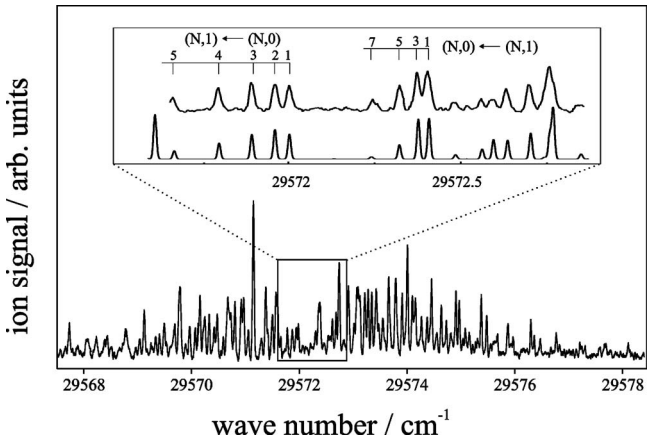

FIG. 11. Rotationally resolved resonance-enhanced two-photon ionization spectrum of the vibrationless $\tilde{A}\,^2A_2'' \leftarrow \tilde{X}\,^2E_1''$ transition in C_5H_5. The inset shows a magnification of the central part of the spectrum, the rotational assignments in the form $(N',K') \leftarrow (N'',K'')$, and a simulation using the parameters reported in Ref. 22.

$$\Gamma' \leftrightarrow \Gamma'' \quad \text{for } \ell_p \text{ even}$$

and

$$\Gamma' \leftrightarrow \Gamma' \quad \text{or } \Gamma'' \leftrightarrow \Gamma'' \quad \text{for } \ell_p \text{ odd}, \tag{20}$$

where Γ represents one of the rovibronic symmetry labels (A_1, A_2, E_1, or E_2) without indication of parity, and ℓ_p designates the angular momentum quantum number of the photoelectron partial wave component. In the transitions considered here, ionization occurs out of one of the π molecular orbitals. The symmetries of the π molecular orbitals are in order of increasing energy a_2'', e_1'', and e_2''. The terms that are allowed in a single-center expansion of these orbitals can be obtained by correlating the irreducible representations of the molecular point group (D_{5h}) to the $D_{\infty h}$ group (taking the C_5 and C_∞ axes to coincide) which gives $\Sigma_u^+ \oplus I_g \oplus I_u$, $\Pi_g \oplus \Pi_u \oplus \Gamma_u$, and $\Delta_u \oplus \Phi_g$, respectively. The dominant terms in the single-center expansion of these orbitals are p_σ, $d_\pi + f_\pi$, and f_δ, respectively. Assuming a single-configuration approximation to be valid, ionization out of the orbitals a_2'', e_1'', and e_2'' would be associated with the selection rules $\Delta K = K^+ - K = (0, \pm 5)$, $(\pm 1, \pm 4)$, and $(\pm 2, \pm 3)$, respectively. The corresponding propensities for the change in the rotational angular momentum quantum number $\Delta N = N^+ - N$ are $(0, \pm 1)$, $(0, \pm 1, \pm 2, \pm 3)$, and $(0, \pm 1, \pm 2, \pm 3)$, if only the leading terms in the single-center expansion of the π orbitals are retained. The spectra shown in Fig. 12 show that the largest observed change in rotational angular momentum amounts to 3 and that smaller changes are not significantly more probable, which rules out a significant contribution of the a_2'' molecular orbital. Moreover, the lowest ionic rotational quantum number amounts to $N^+ = 1$ which implies $\Delta K = \pm 1$. $\Delta K = 0$ can be excluded because the rovibronic symmetry of the $K^+ = 0$ ionic levels would have to be E for a vibronic E symmetry and therefore cannot be accessed from the selected intermediate levels of A_1'' rovibronic symmetry, and every second rotational line would be missing for an A vibronic band (the rovibronic levels of symmetries A_2' and A_2'' have zero spin-statistical weights in $C_5H_5^+$).

This observation indicates that ionization takes place out of the π molecular orbital of symmetry e_1'', i.e., that the observed intensity in the photoelectron spectrum is borrowed from the transition to configuration (ii) defined in Section II A, the mechanism for intensity borrowing being of the Herzberg-Teller type in the cation (see discussion in Sec. II A). The conservation of nuclear spin symmetry dictates that ionic states must have rovibronic symmetry A_1' or A_1''. All consecutive rotational levels in the ion are observed. The vibronic symmetry of the final state must therefore be doubly degenerate because every second rotational level would be missing otherwise (see above).

F. Vibronic calculations

The PFI-ZEKE spectra of C_5H_5 and C_5D_5 were simulated using the vibronic coupling model described in Sec. II. The calculations consisted of a pure PJT model including the $\tilde{a}^+\,{}^1E_2'$ and the $\tilde{b}^+\,{}^1A_1'$ states, their spacing being fixed to the CASSCF(4,5)/cc-pVTZ value of 5600 cm^{-1}. The calculations for $C_5H_5^+$ included the modes ν_{10}, ν_{11}, and ν_{12} with a harmonic oscillator basis with $v_{max} = 13$, 7, and 10, respectively, which sufficed to converge the vibronic eigenvalues up to 2000 cm^{-1} to better than 5 cm^{-1}. The *ab initio* values of the vibrational frequencies and coupling constants were slightly adjusted to improve the agreement with the spectrum, and the resultant values are listed in the last column of Table IV. The simulations of the spectra of $C_5D_5^+$ only included the modes ν_{10} and ν_{11} because the contribution of ν_{12} to the stabilization energy was found to be negligible. A similar observation has been made in the analysis of the $\tilde{X}\,{}^2E_1''$ state of C_5D_5 and was attributed to a rotation of the normal coordinates resulting from the change in mass.[17] The calculations of the spectra of $C_5D_5^+$ were carried out using a vibrational basis with $v_{max} = 20$ and 12 for the modes ν_{10} and ν_{11}, respectively.

A very simple intensity model has been used to calculate the spectra. We have assumed that the normal modes of the intermediate $\tilde{A}\,{}^2A_2''$ and ionic $\tilde{a}^+\,{}^1E_2'$ states are identical to those of the $\tilde{X}^+\,{}^3A_2'$ state and that the Franck-Condon factors for the transition from the $\tilde{A}\,{}^2A_2''$ state to the harmonic oscillator basis states are diagonal. Further, we have assumed that the diabatic electronic transition moment for the transition $\tilde{a}^+\,{}^1E_2' \leftarrow \tilde{A}\,{}^2A_2''$ is unity and that for the transition to the excited singlet state $^1A_1'$ vanishes. This assumption is the translation of the Herzberg-Teller coupling between the "accessible" $^1E_1'$ state of configuration (ii) and the "forbidden" $\tilde{a}^+\,{}^1E_2'$ state of configuration (i) already mentioned at the end of the previous section.

The results of the simulations are compared to the experimental spectra recorded via the $\tilde{A}\,{}^2A_2''$ 0^0, 12^1, and 11^1 intermediate levels for $C_5H_5^+$ [panel (a)] and 0^0 for $C_5D_5^+$ [panel (b)] in Fig. 13. The calculated transitions are labeled according to the vibronic angular momentum quantum number j and a second label u which serves to distinguish different states of the same j. The most striking difference in the spectra of $C_5H_5^+$ and $C_5D_5^+$ is the much smaller spectral density in the spectra of the latter species. This observation is reproduced by the calculations and can thus be attributed to the rotation of normal modes discussed above. The origin band, which is assigned to the band at 69 501 cm^{-1} in $C_5H_5^+$ and at 69 491 cm^{-1} in $C_5D_5^+$ is very weak in the spectra recorded via the 0^0 intermediate level whereas the second band located 71 cm^{-1} above the origin is the dominant feature in both spectra. The intensity ratio of these two lines is inverted when the excitation occurs through the 11^1 or 12^1 levels of the $\tilde{A}\,{}^2A_2''$ state, in good agreement with the calculations. The third band in the spectra of $C_5H_5^+$ (at 69 577 cm^{-1}) is absent in the spectrum of $C_5D_5^+$ and corresponds to the limit of a Rydberg series observed in the photoionization spectrum and is attributed to an excited vibrational level of the $\tilde{X}^+\,{}^3A_2'$ state, most likely the 13^2 level (see Fig. 8). The transition to this level possesses a large Franck-Condon factor because the fundamental frequency ν_{13} of the $\tilde{X}^+\,{}^3A_2'$ ionic state is almost twice that of the $\tilde{A}\,{}^2A_2''$ state.[17] The next higher band is

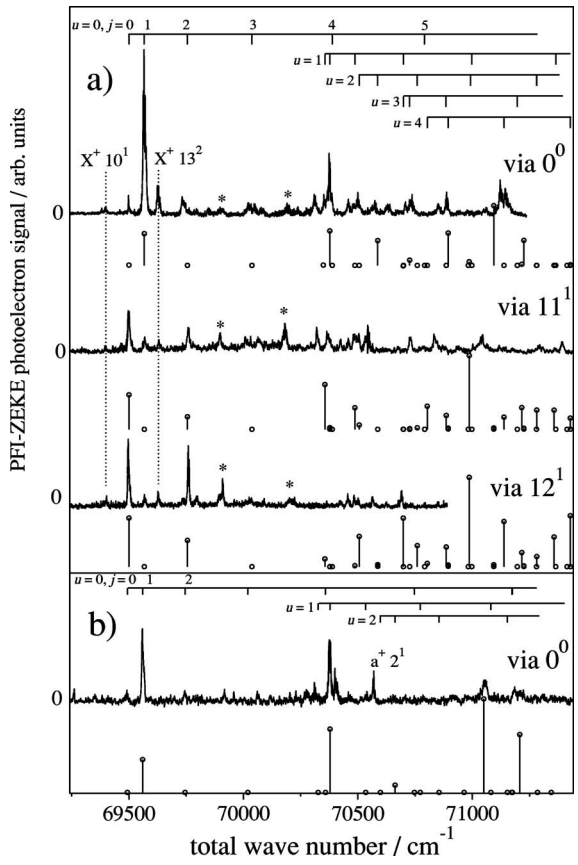

FIG. 13. PFI-ZEKE photoelectron spectra of C_5H_5 (panel a) and C_5D_5 (panel b) recorded following two-photon resonant excitation to the lower component of the $\tilde{a}^+\,^1E_2'$ state via selected vibrational levels of the $\tilde{A}\,^2A_2''$ state. The intermediate level is indicated on the right-hand side above the spectra. The spectra are compared to simulations (vertical stick spectra) of the vibronic structure including the modes ν_{10}, ν_{11}, and ν_{12} in $C_5H_5^+$ and ν_{10} and ν_{11} in $C_5D_5^+$. The bands marked with an asterisk coincide with lines of the precursor C_5H_6 (see Fig. 9).

relatively weak in the excitation via 0^0 but almost as intense as the origin band in the excitation via 12^1 and 11^1, in agreement with the calculations.

Overall, the calculations correctly predict the main features of the experimental spectra, particularly at low energies where calculated and observed positions are in quantitative agreement. The intensity calculations also reproduce several characteristic features of the observed intensity distributions, in particular, the relative intensities of the lowest two transitions and their dependence on the intermediate vibrational level. The main difference between the calculated and measured intensities is that several weak lines in the experimental spectrum are predicted with zero intensity. This discrepancy is a consequence of the (crude) assumption of diagonal Franck-Condon factors in the evaluation of Eq. (18). At higher energies, the agreement between the calculated and experimental spectra deteriorates and the high spectral density prevents conclusive assignments.

The agreement between the calculated and observed spectra of $C_5D_5^+$ is satisfactory. The band at 70 567 cm^{-1} corresponds to a wave number of 1079 cm^{-1} and can be assigned to the 2^1 C–C symmetric stretching mode. The positions of the vibrational bands in the PFI-ZEKE photoelectron spectra of C_5H_5 and C_5D_5 are listed with the corresponding assignments in Tables VI and VII, respectively.

The comparison of the calculated and observed spectra indicates that the origins of the $\tilde{a}^+\,^1E_2'$ ($^1A_1$ component) states have actually been observed at the positions 69 501 cm^{-1} in $C_5H_5^+$ and 69 491 cm^{-1} in $C_5D_5^+$, respectively.

V. DISCUSSION

All electronic states belonging to configuration (i) are accessible in the single-photon VUV experiment. By contrast, ionization from the $\tilde{A}\,^2A_2''$ state of configuration $(a_2'')^1(e_1'')^4(e_2'')^0$ leads to the excited configurations (ii) and (iii) and the states of configuration (i) can only be observed through vibronic or configuration interactions. Since none of the accessible configurations possesses an electronic state of symmetry $^1E_2'$, the transition to the $\tilde{a}^+\,^1E_2'$ state must gain intensity and can only do so by three mechanisms:

(1) The distortion along the e_2' modes mixes the $\tilde{a}^+\,^1E_2'$ state with the $\tilde{b}^+\,^1A_1'$ state and with the $^1E_1'$ state of configuration (ii). Since photoionization to the latter state is allowed, the transition to the $\tilde{a}^+\,^1E_2'$ state becomes allowed by a Herzberg-Teller mechanism. This mechanism cleanly selects the $\tilde{a}^+\,^1E_2'$ state and does not lend intensity to the transitions to the $\tilde{X}^+\,^3A_2'$ state because the *ab initio* data show that the latter is not subject to significant vibronic coupling at low energies. According to this mechanism, the intensity in the spectrum should originate from the transition moment to the diabatic $^1E_2'$ component rather than from that to the $^1A_1'$ component.

(2) The $\tilde{b}^+\,^1A_1'$ state could gain intensity from configuration interaction with the $^1A_1'$ state of configuration (iv). This mechanism would lead to a very different intensity distribution from that expected for the first mechanism because the intensity would be carried by the transition moment to the diabatic $^1A_1'$ component.

(3) Forbidden transitions in photoelectron spectra can gain intensity from allowed ionization channels because of channel interactions in the close-coupling region of the ion-electron complex. Transitions to low members of Rydberg series converging on allowed ionization thresholds can lead to a local enhancement of the intensity of PFI-ZEKE photoelectron spectra and to the observation of forbidden transitions.[43] Such a mechanism is not expected to be highly selective in terms of electronic or vibronic symmetries of the ionic states because the vibronic structure of the collision complex is significantly perturbed by the Rydberg electron. In particular, this mechanism is not expected to be selective either in favor of the $\tilde{a}^+\,^1E_2'$ or the $\tilde{X}^+\,^3A_2'$ state.

The dominant mechanism responsible for the observation of the $\tilde{a}^+\,^1E_2' \leftarrow \tilde{A}\,^2A_2''$ transition can be identified as the first mechanism listed above by considering the vibrational intensity distributions in the spectra and the results of the rotationally resolved measurements. The latter indeed

directly indicate the mixing of configuration (ii) (see Sec. IV E). In the simulations of vibrational intensities, we have assumed that the only nonvanishing transition moment is that to the diabatic $^1E_2'$ component, which has explained the observed intensity distributions in the two lowest bands and their dependence on the intermediate level. In model calculations relying on a strong transition moment to the $^1A_1'$ component, the intensity pattern in these lowest bands was found to be inverted. The second mechanism can thus be ruled out.

The third mechanism also contributes to the observed intensity pattern. The absence of a sharp onset of the photoionization signal at the $\tilde{X}^+\,^3A_2'$ threshold indicates a negligible direct ionization to the $^3A_2'$ state. However, the structured photoionization signal between the $^3A_2'$ origin and 69 567 cm^{-1} is attributed to electronic autoionization of low-n Rydberg states belonging to series converging on electronically excited states of the cation into the continua associated with the $\tilde{X}^+\,^3A_2'$ state. The interaction of these low Rydberg states with Rydberg states belonging to series converging on vibrationally excited levels of the $\tilde{X}^+\,^3A_2'$ state leads to the observation of Rydberg series in both C_5H_5 and C_5D_5 (see Fig. 8). These Rydberg series converge to thresholds that we have tentatively assigned to overtones of out-of-plane vibrations (ν_{13} in $C_5H_5^+$ and ν_8 in $C_5D_5^+$) of the $\tilde{X}^+\,^3A_2'$ state. The out-of-plane vibrations enhance spin-orbit coupling in the cyclopentadienyl cation.[44] This effect could explain the observation of these vibrational levels by an interaction between the $\tilde{X}^+\,^3A_2'$ and $\tilde{a}^+\,^1E_2'$ states mediated by spin-orbit coupling. An additional factor favoring the observation of the out-of-plane vibrations is the large change of their frequencies between the $\tilde{A}\,^2A_2''$ and the $\tilde{X}^+\,^3A_2'$ states (see Refs. 2 and 16).

The *ab initio* calculations of the cuts of the potential energy surface along the vibrational modes of symmetry e_2' show that the potential energy surface of the $\tilde{X}^+\,^3A_2'$ state crosses the surface of the $\tilde{a}^+\,^1E_2'$ state near to its minimum (see right-hand-side panel of Fig. 1). Although spin-orbit effects are relatively small in hydrocarbon molecules, they may nevertheless lead to an interaction of the singlet and triplet states of $C_5H_5^+$ and to avoided crossings between the surfaces associated with different spin multiplicities. This interaction may cause perturbations of the vibronic structure in the $\tilde{a}^+\,^1E_2'$ state and significant intersystem-crossing rates for the $\tilde{a}^+\,^1E_2'$ state. The inclusion of these effects in the vibronic calculations is beyond the scope of the present investigation but must certainly be considered in a more detailed theoretical analysis.

The remaining discrepancies between the calculated and observed vibronic structure can have several origins. The restriction of the dynamic calculations to 3 (2) PJT active modes in $C_5H_5^+$ ($C_5D_5^+$), which was imposed by the large dimension of the basis set required to converge the calculations, represents the most stringent approximation. In the case of a very large distortion, anharmonicities in the potential surfaces may play an important role and the use of a harmonic oscillator basis may become questionable. The choice of normal coordinates for the vibronic calculations could be improved by deriving them from detailed calculations of the singlet potential energy surfaces instead of using the normal modes of the triplet state.

VI. CONCLUSIONS

The results of our investigations of the cyclopentadienyl cation by high-resolution photoelectron spectroscopy and *ab initio* quantum chemical calculations can be summarized as follows:

(i) The cyclopentadienyl cation possesses a ground electronic state of symmetry $^3A_2'$ with a D_{5h} minimum energy structure.

(ii) The first excited electronic state of symmetry $^1E_2'$ is subject to a strong PJT interaction with the next higher singlet state of symmetry $^1A_1'$ which stabilizes the lower state by $\sim$4000 cm^{-1}.

(iii) The adiabatic ionization energies corresponding to the formation of the $\tilde{X}^+\,^3A_2'$ and $\tilde{a}^+\,^1E_2'$ states are 67 967±4 and 69 501±4 cm^{-1}, respectively, so that the singlet-triplet interval amounts to 1534±6 cm^{-1}. As discussed in Ref. 45, this interval is a key quantity in the characterization of diradicals and an important test for the quality of *ab initio* calculations.

(iv) The $\tilde{a}^+\,^1E_2' \leftarrow \tilde{A}\,^2A_2''$ photoionizing transition, which is forbidden in the single-configuration approximation, has been observed in our resonance-enhanced two-photon experiments because of a Herzberg-Teller interaction with the excited $^1E_1'$ state which is mediated by the JT active e_1' and the PJT active e_2' modes. Since the latter are responsible for a strong geometric distortion, their contribution is likely to be dominant.

(v) In the $D_{5h}(M)$ molecular symmetry group, the linear JT (PJT) and quadratic JT (PJT) interactions are restricted by symmetry to distinct sets of vibrational modes. Since the PJT stabilization dominates largely over the linear JT stabilization, the nuclear motion in the lowest vibronic levels of $C_5H_5^+$ can be described by treating the e_2' modes only. This is in contrast to a recent analysis,[3] in which the authors suggested that the distortion of $C_5H_5^+$ could be understood in terms of a linear JT effect and that the nuclear motion encircled *six* conical intersections. Although the latter statement may apply to excited vibronic levels lying close to the location of the electronic degeneracies, our experiments provide no evidence for the validity of the former.

(vi) The weakness of the linear JT effect in the $\tilde{a}^+\,^1E_2'$ state confirms the general rule derived by Ceulemans[26] and Watson,[27] that the linear JT effect vanishes in an electronic state containing an even number of electrons in e orbitals. This result has an interesting consequence for antiaromatic molecules: Since they possess $4n$ electrons in π molecular orbitals, the linear JT effect is expected to be negligible in all of their low-lying electronic states and vibronic coupling will thus be dominated by the PJT effect. In the special case of the molecules with $D_{4nh}(M)$ symmetry, the linear $E\otimes e$ JT effect is inexistent anyway

because the electronic states resulting from the most stable electronic configuration are nondegenerate (since $E \otimes E$ does not contain any degenerate representation in these groups).

(vii) The crossing of the singlet and triplet surfaces occurs close to the minimum of the lowest singlet surface. Vibrational perturbations are a probable consequence and a possible explanation for the complexity of the observed vibronic structure at higher energies. The cyclopentadienyl cation may thus represent an interesting test case for studying the joint effects of vibronic coupling and an intersystem crossing.

ACKNOWLEDGMENTS

The authors thank Professor H. Köppel, and Professor L. Cederbaum (Heidelberg), and Professor S. Mahapatra (Hyderabad) for several useful discussions, and Guido Grassi (ETH Zürich) for the synthesis of deuterated cyclopentadiene (C_5D_6). This work is supported financially by the Swiss National Science Foundation under Project No. 200020–116245 and the ETH Zürich.

[1] W. T. Borden and E. R. Davidson, J. Am. Chem. Soc. **101**, 3771 (1979).
[2] E. P. F. Lee and T. G. Wright, Phys. Chem. Chem. Phys. **1**, 219 (1999).
[3] S. Zilberg and Y. Haas, J. Am. Chem. Soc. **124**, 10683 (2002).
[4] A. D. Allen, M. Sumonja, and T. T. Tidwell, J. Am. Chem. Soc. **119**, 2371 (1997).
[5] I. B. Bersuker, *The Jahn-Teller Effect* (Cambridge University Press, Cambridge, UK, 2006).
[6] F. P. Lossing and J. C. Traeger, J. Am. Chem. Soc. **97**, 1579 (1975).
[7] H. Schwarz, H. Thies, and W. Franke, in *Ionic Processes in the Gas Phase*, edited by M. A. A. Ferreira (Reidel, Dordrecht, 1984), pp. 267–286.
[8] M. Saunders, R. Berger, A. Jaffe *et al.*, J. Am. Chem. Soc. **95**, 3017 (1973).
[9] E. Wasserman and R. S. Hutton, Acc. Chem. Res. **10**, 27 (1977).
[10] H. J. Wörner and F. Merkt, Angew. Chem., Int. Ed. **45**, 293 (2006).
[11] W. J. Hehre and P. von Ragué Schleyer, J. Am. Chem. Soc. **95**, 5837 (1973).
[12] M. N. Glukhovtsev, B. Reindl, and P. von Ragué Schleyer, Mendeleev Commun. **3**, 100 (1993).
[13] J. Feng, J. Leszczynski, B. Weiner, and M. C. Zerner, J. Am. Chem. Soc. **111**, 4648 (1989).
[14] H. Köppel, W. Domcke, and L. S. Cederbaum, Adv. Chem. Phys. **57**, 59 (1984).
[15] H. Köppel, L. S. Cederbaum, and W. Domcke, J. Chem. Phys. **89**, 2023 (1988).
[16] B. E. Applegate, T. A. Miller, and T. A. Barckholtz, J. Chem. Phys. **114**, 4855 (2001).
[17] B. E. Applegate, A. J. Bezant, and T. A. Miller, J. Chem. Phys. **114**, 4869 (2001).
[18] H. von Busch, V. Dev, H. A. Eckel, S. Kasahara, J. Wang, W. Demtröder, P. Sebald, and W. Meyer, Phys. Rev. Lett. **81**, 4584 (1998); **82**, 3560(E) (1999).
[19] H. J. Wörner, R. van der Veen, and F. Merkt, Phys. Rev. Lett. **97**, 173003 (2006).
[20] M. V. Berry, Proc. R. Soc. London, Ser. A **392**, 45 (1984).
[21] U. Öpik and M. H. L. Pryce, Proc. R. Soc. London, Ser. A **238**, 425 (1957).
[22] L. Yu, S. C. Foster, J. M. Williamson, M. C. Heaven, and T. A. Miller, J. Phys. Chem. **92**, 4263 (1988).
[23] W. T. Borden, *Diradicals* (Wiley, New York, 1982).
[24] P. C. Engelking and W. C. Lineberger, J. Chem. Phys. **67**, 1412 (1977).
[25] T. A. Barckholtz and T. A. Miller, Int. Rev. Phys. Chem. **17**, 435 (1998).
[26] A. Ceulemans, Chem. Phys. **66**, 169 (1982).
[27] J. K. G. Watson, Mol. Phys. **96**, 1721 (1999).
[28] R. Meiswinkel and H. Köppel, Chem. Phys. Lett. **201**, 449 (1993).
[29] W. E. Ernst and S. Rakowsky, Phys. Rev. Lett. **74**, 58 (1995).
[30] D. T. Vituccio, O. Golonzka, and W. E. Ernst, J. Mol. Spectrosc. **184**, 237 (1997).
[31] F. Merkt, A. Osterwalder, R. Seiler, R. Signorell, H. Palm, H. Schmutz, and R. Gunzinger, J. Phys. B **31**, 1705 (1998).
[32] S. Willitsch, J. M. Dyke, and F. Merkt, Helv. Chim. Acta **86**, 1152 (2003).
[33] U. Hollenstein, H. Palm, and F. Merkt, Rev. Sci. Instrum. **71**, 4023 (2000).
[34] *M.I.T. Wavelength Tables: Wavelengths by Element*, edited by F. M. Phelps III (MIT Press, Cambridge, MA, 1982), Vol. 2.
[35] G. Reiser, W. Habenicht, K. Müller-Dethlefs, and E. W. Schlag, Chem. Phys. Lett. **152**, 119 (1988).
[36] H.-J. Werner, P. J. Knowles, R. Lindh *et al.*, MOLPRO, version 2002.6, a package of *ab initio* programs, 2002.
[37] P. Garcia-Fernandez, I. B. Bersuker, and J. E. Boggs, J. Chem. Phys. **125**, 104102 (2006).
[38] G. Herzberg and H. C. Longuet-Higgins, Discuss. Faraday Soc. **35**, 77 (1963).
[39] A. D. Buckingham, B. J. Orr, and J. M. Sichel, Philos. Trans. R. Soc. London, Ser. A **268**, 147 (1970).
[40] S. Willitsch and F. Merkt, Int. J. Mass. Spectrom. **245**, 14 (2005).
[41] L. Yu, J. M. Williamson, and T. A. Miller, Chem. Phys. Lett. **162**, 431 (1989).
[42] R. Signorell and F. Merkt, Mol. Phys. **92**, 793 (1997).
[43] F. Merkt and T. P. Softley, Int. Rev. Phys. Chem. **12**, 205 (1993).
[44] Y. Shiota, M. Kondo, and K. Yoshizawa, J. Chem. Phys. **115**, 9243 (2001).
[45] W. T. Borden and E. R. Davidson, Acc. Chem. Res. **14**, 69 (1981).